Quantum-spin-liquid states in the two-dimensional kagome antiferromagnets $Zn_xCu_{4-x}(OD)_6Cl_2$

S.-H. LEE[1]*, H. KIKUCHI[2], Y. QIU[3], B. LAKE[4,5], Q. HUANG[3], K. HABICHT[4] AND K. KIEFER[4]

[1]Department of Physics, University of Virginia, Charlottesville, Virginia 22904-4714, USA
[2]Department of Applied Physics, University of Fukui, Fukui 910-8507, Japan
[3]NIST Center for Neutron Research, National Institute of Standards and Technology, Gaithersburg, Maryland 20899, USA
[4]Hahn–Meitner-Institut, Glienicker Straße 100, Berlin D-14109, Germany
[5]Institut für Festkörperphysik, Technische Universität Berlin, Hardenbergstr. 36, 10623 Berlin, Germany
*e-mail: shlee@virginia.edu

Published online: 26 August 2007; doi:10.1038/nmat1986

A three-dimensional system of interacting spins typically develops static long-range order when it is cooled. If the spins are quantum ($S = 1/2$), however, novel quantum paramagnetic states may appear. The most highly sought state among them is the resonating-valence-bond state[1,2], in which every pair of neighbouring quantum spins forms an entangled spin singlet (valence bonds) and these singlets are quantum mechanically resonating among themselves. Here we provide an experimental indication for such quantum paramagnetic states existing in frustrated antiferromagnets, $Zn_xCu_{4-x}(OD)_6Cl_2$, where the $S = 1/2$ magnetic Cu^{2+} moments form layers of a two-dimensional kagome lattice. We find that in $Cu_4(OD)_6Cl_2$, where distorted kagome planes are weakly coupled, a dispersionless excitation mode appears in the magnetic excitation spectrum below ~20 K, whose characteristics resemble those of quantum spin singlets in a solid state, known as a valence-bond solid, that breaks translational symmetry. Doping with non-magnetic Zn^{2+} ions reduces the distortion of the kagome lattice, and weakens the interplane coupling but also dilutes the magnetic occupancy of the kagome lattice. The valence-bond-solid state is suppressed, and for $ZnCu_3(OD)_6Cl_2$, where the kagome planes are undistorted and 90% occupied by the Cu^{2+} ions, the low-energy spin fluctuations become featureless.

The resonating-valence-bond (RVB) state was originally introduced in the early 1970s as a possible ground state for two-dimensional triangular quantum antiferromagnets[1,2]. A decade later, the formation of the RVB state was proposed as a mechanism for high-temperature superconductivity[3]. Since then, such quantum-spin-liquid (QSL) states have been greatly sought after in various strongly correlated electron systems. Theoretically, substantial progress has been made on the physics of quantum paramagnets[4–10]. For instance, it has been shown that there exists another simpler type of cooperative quantum state known as a valence-bond solid (VBS), in which each spin forms a spin singlet ($|\uparrow\downarrow\rangle - |\downarrow\uparrow\rangle$) or valence bond with a neighbour, resulting in an ordered pattern (solid) of valence bonds. It is not easy, however, to find QSLs in real systems, because these states lack static order and their dynamic order parameters are hard to observe: for the VBS state these are the gapped $S = 1$ magnon excitations, and for the RVB state these are an exotic gapless continuum of excitations with fractional spin $S = 1/2$. Such states in systems with spatial dimensions larger than one have so far eluded all experimental attempts. Over the last two decades or so, frustrated magnets have been studied as excellent systems to look for such QSLs because of their intrinsic macroscopic ground-state degeneracy[11,12].

Recently, $Zn_xCu_{4-x}(OD)_6Cl_2$ has been proposed as an ideal candidate for the quantum ($S = 1/2$) kagome system, where quantum spins form a two-dimensional network of corner-sharing triangles[13–16] (see Fig. 1c). We have made elastic- and inelastic-neutron-scattering measurements on this compound with various Zn concentrations ($x = 0, 0.2, 0.4, 0.66, 1.0$) and studied how the static and dynamic spin correlations evolve with x and temperature T. For $x = 0$, $Cu_4(OD)_6Cl_2$, where the kagome layers are weakly coupled via Cu^{2+} ions at the triangular sites located in between the Cu^{2+} kagome layers, our data show two nearly dispersionless modes of magnetic excitations at energy transfers $\hbar\omega_1 = 1.3$ meV and $\hbar\omega_0 = 7$ meV, respectively (see Supplementary Information, Figs S1,S2). This system undergoes magnetic long-range (Néel) order. Figure 2a shows that magnetic Bragg peaks develop below the Néel temperature $T_N \sim 7$ K with a characteristic wavevector of (010) with respect to the $P2_1/n$ crystal symmetry[17]. This transition is consistent with the previously reported bulk susceptibility data[17,18]. The magnetic structure, refined using the elastic data, is shown in Fig. 1c (for details, see the caption of Fig. 2a and the Supplementary Information). Interestingly, the spins are not 120° apart from each other as expected in the so-called $q = 0$ or $\sqrt{3} \times \sqrt{3}$ spin structures proposed as the possible ground states of a kagome antiferromagnet. Instead, they are collinear, the implication of which will be discussed later. As the static order sets in, on cooling, the low-energy spectrum below 2.5 meV starts to develop a gap (Fig. 2b) and the gap, $\hbar\omega_1$, increases as the static moment $\langle M \rangle$ increases. It is well known that a Néel state with a single ion anisotropy develops a gap in some long-ranged spin-wave excitation modes[19]. For example, in the $q = 0$ kagome Néel state, a zero-energy mode that involves swinging of spins about a bisecting axis of symmetry can be lifted in energy by an anisotropy[20,21]. We conclude that the $\hbar\omega_1$ mode is due to such nearly dispersionless spin-wave excitations allowed by the Néel state of $Cu_4(OD)_6Cl_2$.

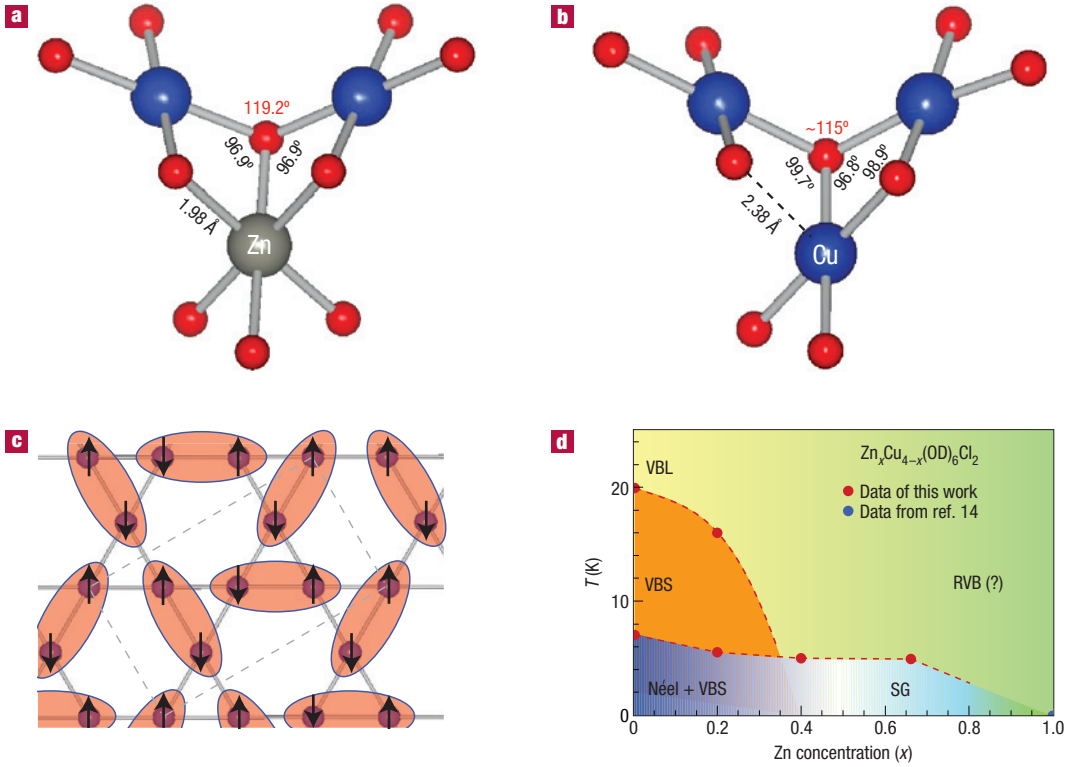

Figure 1 Local crystal structure and phase diagram of $Zn_xCu_{4-x}(OD)_6Cl_2$. **a**, Local environments around the non-magnetic Zn^{2+} ion (grey spheres) at the triangular site and the magnetic Cu^{2+} ions (blue spheres) at the neighbouring kagome sites. The kagome Cu^{2+} ions are surrounded by four O^{2-} (red spheres) and two Cl^- ions in a distorted octahedral environment with an elongation along the Cl^- axis. Here, for simplicity, only O^{2-} ions are shown. The Zn^{2+} ion is surrounded by six O^{2-} ions in a perfect octahedral environment. **b**, Local oxygen environments around the triangular site when the Zn^{2+} ion is replaced by a magnetic Cu^{2+} ion. Because a Cu^{2+} ion is Jahn–Teller active, its oxygen octahedron distorts. The Cu^{2+}—O^{2-} bonds where the wavefunctions of their unpaired electrons overlap are shown by grey bars. The superexchange interaction between nearest-neighbouring Cu^{2+} moments mediated via oxygen is very sensitive to the Cu–O–Cu bond angle, θ, and it changes from strongly antiferromagnetic when $\theta = 180^\circ$ to zero when $\theta \approx 95^\circ$ to ferromagnetic when $\theta < 95^\circ$ (refs 26,27). These angles are shown in the figure and indicate that interactions between the kagome Cu^{2+} and the doped triangular Cu^{2+} spins are weak, which makes the Cu^{2+} moments at the triangular sites almost independent spins and thus makes $Zn_xCu_{4-x}(OD)_6Cl_2$ a weakly coupled kagome system for all Zn concentrations x. **c**, The spin structure of $Cu_4(OD)_6Cl_2$ determined by fitting our elastic-neutron-scattering data shown in the inset of Fig. 2a to a model of kagome spins only (see the caption of Fig. 2a for the details). The spins are collinear with each other: the up and down arrows represent antiparallel spins in the Néel state $T < T_N = 7$ K. The kagome lattice is slightly distorted in $Cu_4(OD)_6Cl_2$ to have two bond lengths, 3.41 and 3. 42 Å. The neighbouring spins with the shorter bond length are antiparallel whereas those with the longer bond length are parallel. The dashed lines represent the chemical and magnetic unit cell. The ovals represent the quantum singlets $(|\uparrow\downarrow\rangle - |\downarrow\uparrow\rangle)$ in the VBS state of $Cu_4(OD)_6Cl_2$, $T < T_c = 20$ K. **d**, Phase diagram of $Zn_xCu_{4-x}(OD)_6Cl_2$ as a function of temperature and doping. The term Néel +VBS is supposed to describe how the Néel state contains the antiparallel spin alignment found in the higher-temperature VBS state around the dominant exchange interactions of the distorted lattice.

This explanation is supported by the doping effect of non-magnetic Zn^{2+} ions. The Néel order weakens on Zn doping, and disappears somewhere between $x = 0.4$ and 0.66 (Fig. 3a). The $\hbar\omega_1$ mode is present as long as the Néel order is present (Fig. 3b), but it shifts to lower energies as the ordered moment decreases. In a similar way the $\hbar\omega_1$ decreases as temperature increases in the $x = 0$ sample (Fig. 2b). This is because the ordered moment decreases with T ($< T_N$) (see Fig. 2a).

The $\hbar\omega_0 = 7.2$ meV mode of the $x = 0$ system, in contrast to the $\hbar\omega_1$ mode, exists up to $T_c \sim 20$ K, which is well above its Néel phase ($T_N = 7$ K) (red circles in Fig. 2a). Indeed, previous specific-heat, bulk-susceptibility[17] and muon-spin-resonance measurements[16] indicated a transition at ~18 K. This confirms that the development of the $\hbar\omega_0$ mode below T_c represents a phase transition between two different states. The question that arises is what kind of states they are. The value of $\hbar\omega_0$ does not change below T_c (the right-hand side of Fig. 2b), which starkly contrasts with the behaviour of the $\hbar\omega_1$ mode below T_N. In addition, the momentum (Q) dependence of the $\hbar\omega_0$ mode has a peak at 1.1 $Å^{-1}$, which is different from that of the $\hbar\omega_1$ mode, which has a peak at ~0.6 $Å^{-1}$ (Fig. 4a). These facts clearly tell us that the $\hbar\omega_0$ mode is not related to any spin wave of the Néel state.

The origin of the $\hbar\omega_0 = 7.2$ meV mode can be elucidated by its Q dependence. As shown in Fig. 4a, the Q dependence of the $\hbar\omega_0$ mode (red circles) resembles that of the singlet-to-triplet excitations of spin dimers (red line), $1 - (\sin(Qr_0)/Qr_0)$ (refs 22,23), with $r_0 = 3.41$ Å, which is the distance between the nearest-neighbour Cu^{2+} ($S = 1/2$) ions in the kagome lattice. Furthermore, the mode energy $\hbar\omega_0 = 7.2$ meV is close to the estimated coupling constant for $Cu_4(OD)_6Cl_2$, $J \sim 9.7$ meV from bulk susceptibility data. A recent study[24] fitted the data of $Zn_xCu_{4-x}(OD)_6Cl_2$ with $x = 1$ to a kagome lattice Heisenberg model using a numerical linked-cluster method and yielded $J = 170$ K $= 14.6$ meV for $x = 1$. It is reported that the Curie–Weiss temperature decreases when the Zn concentration decreases[13]. If we scale the coupling constant accordingly, we obtain $J \sim 9.7$ meV for

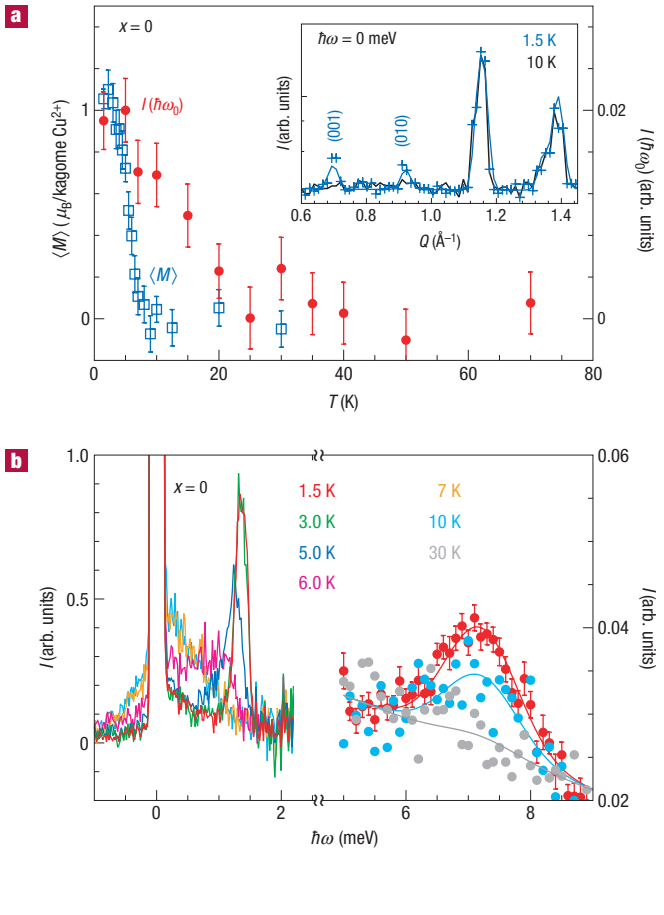

Figure 2 Energy and temperature dependence of the static and dynamic spin correlations in $Cu_4(OD)_6Cl_2$. a, The inset shows elastic-neutron-scattering patterns obtained from a powder sample at 1.5 K (blue plus symbols) and 10 K (black line). Magnetic Bragg peaks, such as the (001) and (010) reflections, exist at 1.5 K, indicating the development of Néel order at low temperatures. The magnetic Bragg peaks could be reproduced by considering kagome spins only with an ordered moment, $\langle M\rangle_{\text{kagome}}$, of $1.15\pm0.15\ \mu_B/Cu^{2+}$. The data could also be fitted equally well by considering both kagome and triangular spins with $\langle M\rangle_{\text{kagome}}=1.07\pm0.20\ \mu_B/Cu^{2+}$ and $\langle M\rangle_{\text{triangular}}=0.59\pm0.45\ \mu_B/Cu^{2+}$, respectively. The fact that the kagome spins are sufficient to reproduce the data and that $\langle M\rangle_{\text{triangular}}\sim0.5\,\langle M\rangle_{\text{kagome}}$ when the triangular spins are included supports our speculation from the crystal structure that the interactions between the kagome and triangular spins are very weak. The blue line in this inset and the collinear spin structure shown in Fig. 1c are the results obtained with the model of the kagome spins only. The main part **a** shows the detailed temperature dependence of $\langle M\rangle_{\text{kagome}}$ (blue squares) and that of the $\hbar\omega_0=7.2$ meV mode intensity (red circles). **b**, Magnetic-excitation spectrum of $Cu_4(OD)_6Cl_2$ at several different temperatures, obtained by integrating over Q data similar to those shown in Supplementary Information, Fig. S1. Errors were determined statistically by the Poisson distribution; that is, they are the square roots of the intensities.

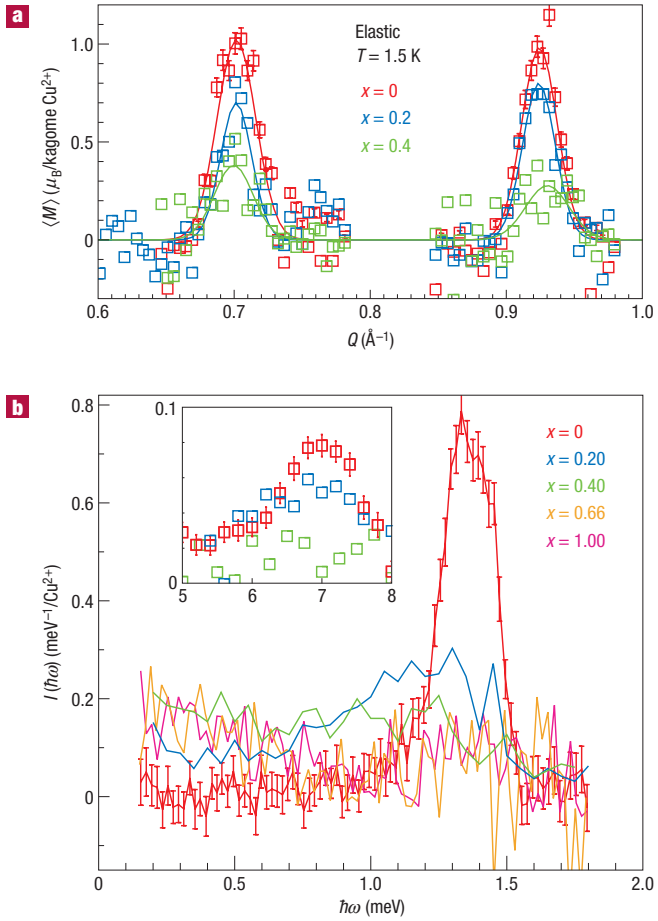

Figure 3 Doping dependence of static and dynamic spin correlations. **a**, Elastic-neutron-scattering intensities at two magnetic reflections obtained for $Zn_xCu_{4-x}(OD)_6Cl_2$ with $x=0$, 0.2 and 0.4 and at 1.5 K. **b**, Magnetic-excitation spectrum in $Zn_xCu_{4-x}(OD)_6Cl_2$ with $x=0$, 0.2, 0.4, 0.66 and 1.0 measured at 1.5 K. Statistical errors were determined by the Poisson distribution.

$x=0$. These facts strongly indicate that the $\hbar\omega_0$ mode is the gapped $S=1$ quasiparticle excitation that is the hallmark of a VBS state. We believe that the VBS state arises owing to the lattice distortion, which results in broken translational symmetry and non-uniform interactions in the kagome plane. The valence-bond singlets form around the dominant interactions and the excitations correspond to promoting one of these into an $S=1$ triplet. On further cooling, the spins freeze into a collinear Néel state rather than the non-collinear arrangements (for example $q=0$ or $\sqrt{3}\times\sqrt{3}$) commonly found in frustrated kagome antiferromagnets. This ordering retains the antiparallel spin alignment within the original singlets established at higher temperatures in the VBS state. Above T_c, the $\hbar\omega_0$ mode disappears and is replaced by a featureless energy continuum. Interestingly, however, the Q dependence of the low-energy continuum above T_c (black circles in Fig. 4a) is the same as that of the $\hbar\omega_0$ mode. In other words, the spin-liquid phase above T_c has energy-continuum excitations with the Q dependence of spin dimers, identifying this as a valence-bond liquid. On doping with the non-magnetic Zn^{2+} ions, T_c decreases and the $\hbar\omega_0$ mode weakens, and for $x=0.4$ it disappears altogether (see Fig. 3b). It is to be noted that the crystal symmetry changes at $x=0.33$ from monoclinic $P2_1/n$ ($x<0.33$) to rhombohedral $R\bar{3}m$ ($x>0.33$) (ref. 13), which coincides with the disappearance of the VBS state and the dramatic weakening of the Néel order.

For $x\geq0.66$, when there is no Néel order, the low-energy excitations become gapless and also weaken considerably, in agreement with previous measurements on $x=1$ (ref. 14), and this makes the investigation non-trivial. To observe any increase in low-energy spin fluctuations on cooling for $x=0.66$, we subtracted the data measured at 10 K from the 1.5 K data. The difference, $\int_{0.2\text{ meV}}^{0.8\text{ meV}} I(1.5\,\text{K})-I(10\,\text{K})\,\mathrm{d}(\hbar\omega)$ (blue squares in Fig. 4b), shows a broad peak centred at $Q\sim0.8\,\text{Å}^{-1}$, halfway

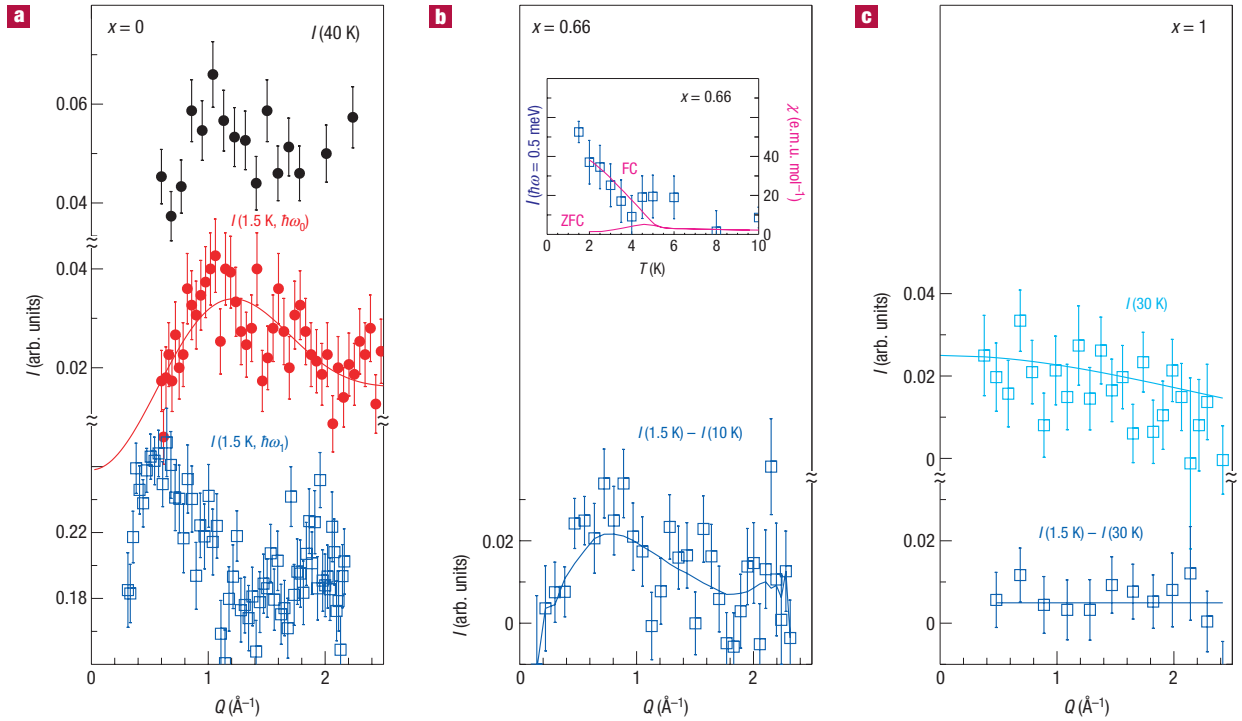

Figure 4 ***Q*** **dependence of magnetic fluctuations in $Zn_xCu_{4-x}(OD)_6Cl_2$.** **a**, $Cu_4(OD)_6Cl_2$; **b**, $Zn_{0.66}Cu_{3.34}(OD)_6Cl_2$; **c**, $ZnCu_3(OD)_6Cl_2$. Different colours represent the data obtained for different energies at different temperatures. In **a**, black symbols represent I ($T = 40$ K, $\hbar\omega = 4$ meV), red I ($T = 1.5$ K, $\hbar\omega_0$) and blue I ($T = 40$ K, $\hbar\omega_1$). **b**, $\int_{0.2\ \mathrm{meV}}^{0.8\ \mathrm{meV}} I\,(1.5\,\mathrm{K}) - I\,(10\,\mathrm{K})\,\mathrm{d}(\hbar\omega)$ (blue squares) obtained from the $x = 0.66$ sample, which shows an increase of intensity at low energies below 10 K. The inset of **b** shows the temperature dependence of these low-energy excitations (blue squares) and that of the bulk susceptibility (pink lines) measured under field-cooled (FC) and zero-field-cooled (ZFC) conditions, indicating spin freezing below 5 K. **c**, Low-energy magnetic excitations measured at 30 K and with $\hbar\omega = -0.6$ meV (cyan squares). Here I (1.5 K) with negative energy transfer was measured to determine non-magnetic contributions using the principle of detailed balance, $I(-\omega) = \exp(-\hbar\omega/k_BT)I(\omega)$, where k_B is the Boltzmann factor, and was subtracted from I (30 K). Blue squares are the difference in intensity between 1.5 and 30 K, measured with $\hbar\omega = 0.6$ meV. Statistical errors were determined by the Poisson distribution.

between the two magnetic (001) and (010) Bragg peak positions of the $x = 0$ system (see Fig. 3a), suggesting that this intensity is due to short-range critical fluctuations around the Néel state. The low-energy excitations grow below $T_f \sim 5$ K (blue squares in the inset of Fig. 4), at which bulk-susceptibility (χ) data (magenta lines) show field-cooled and zero-field-cooled hysteresis, indicating a spin-glass-like phase transition. When $x = 1$, on the other hand, not even spin freezing occurs at low temperatures. Only a nearly Q-independent increase is observed on cooling at low temperatures (blue squares in Fig. 4c). Interestingly, the Q dependence of low-energy magnetic excitations (cyan squares) can be modelled by the squared magnetic form factor of the single Cu^{2+} ion with $S = 1/2$ (cyan line). This behaviour, characteristic of the excitations of uncoupled spins, is also observed in the magnetic-field-induced excitations of the spin-liquid phase of $Zn_xCu_{4-x}(OD)_6Cl_2$ with $x \geq 0.66$. As shown in Fig. 5, when the field, H, is applied to the $x = 0.66$ sample, the energy continuum of magnetic excitations changes to develop an excitation mode at finite energies. The peak energy of the field-induced excitation is proportional to H: E (meV) $= 0.12(3)H$ (T) $\approx g\mu_B H$, where g is the g factor and μ_B is the Bohr magneton, which is the expected Zeeman splitting behaviour of a single magnetic ion in the presence of an external magnetic field. This result is consistent with the previously observed field effect on the $x = 1$ sample[14].

What is the origin of the single-ionic excitations in the spin-liquid phase of $Zn_xCu_{4-x}(OD)_6Cl_2$ with $x \geq 0.66$? Spin-liquid states that have been theoretically proposed for the perfect quantum kagome antiferromagnet have strong characteristic Q dependences due to strong spin correlations, which cannot explain the observed single-ionic behaviour. To understand the observed behaviour let us consider the effect of Zn doping on the crystal structure. It has been assumed that because the Zn^{2+} ions are not Jahn–Teller active they prefer the triangular sites, which are surrounded octahedrally by six O^{2-} ions, over the kagome sites, which are surrounded non-octahedrally by four O^{2-} and two Cl^{2-} ions (see Fig. 1a,b). If the non-magnetic Zn^{2+} ions replace the Cu^{2+} ions at the triangular sites only, but leave the Cu^{2+} ions at the kagome sites intact, $ZnCu_3(OD)_6Cl_2$ would be the fully occupied perfect two-dimensional quantum-spin kagome system. To find out whether this is indeed the case, we have made neutron powder-diffraction measurements on the $x = 1$ sample and refined the crystal structure. Our results show that Zn^{2+} ions prefer the octahedral triangular sites but they can also go into the non-octahedral kagome sites. For $x = 1$ the triangular sites are 36% occupied by Cu^{2+} ions and 64% by Zn^{2+} ions whereas the kagome sites are 90% occupied by Cu^{2+} ions and 10% by Zn^{2+} ions (see the Supplementary Information). The dilution of the kagome lattice may provide a possible explanation for the single-ionic spin fluctuations.

To test this scenario we have normalized our inelastic-neutron-scattering data to an absolute unit by comparing the magnetic intensity with the intensities of nuclear peaks (S.-H. Lee, unpublished) (see Figs 3b and 5). For $x = 0$ and at 1.5 K, the integrated intensity of the $\hbar\omega_1 = 1.3$ meV mode, $\int_{1\ \mathrm{meV}}^{1.7\ \mathrm{meV}} I(\hbar\omega)\,\mathrm{d}(\hbar\omega) = 0.20(2)/Cu^{2+}$,

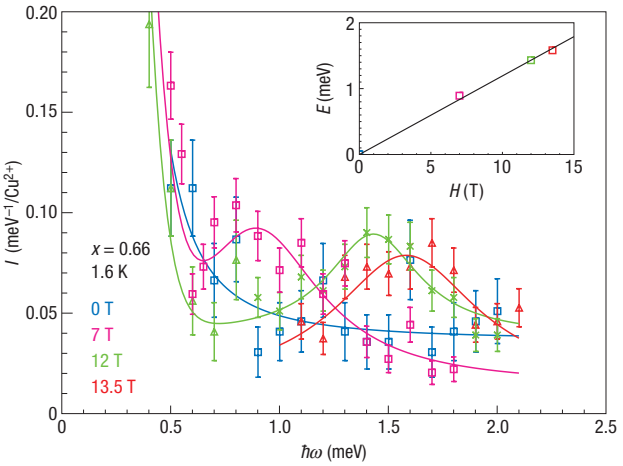

Figure 5 Magnetic-field effect on magnetic excitations. Magnetic-excitation spectrum observed from a powder sample of $Zn_{0.66}Cu_{3.34}(OD)_6Cl_2$ with application of various external magnetic fields, $H = 0, 7, 12$ and 13.5 T. The inset shows the peak energy E of the field-induced excitations as a function of H. Statistical errors were determined by the Poisson distribution.

which corresponds to 27% of the total magnetic scattering cross-section, $S(S+1) = 0.75/Cu^{2+}$. For $x = 0.66$ and 1, the integrated intensity over low energies up to 1.7 meV is $\int_{0.2\,meV}^{1.7\,meV} I(\hbar\omega)\,d(\hbar\omega) = 0.11(3)/Cu^{2+}$ and $0.13(3)/Cu^{2+}$, respectively, assuming that all Cu^{2+} ions are involved. If we assume that only the unpaired triangular Cu^{2+} ions are involved, the integrated intensity for $x = 1$ becomes $1.1(2)/Cu^{2+}$, which is larger than $S(S+1)/Cu^{2+}$ and thus unrealistic. This indicates that the single-ionic low-energy excitations observed in the spin-liquid phase for $x = 0.66$ and 1 are indeed due to collective excitations of kagome Cu^{2+} ions. It is possible that the valence-bond-liquid state observed for $x = 0$ evolves, on increasing x, into a similar spin-liquid state but with much shorter-range spin correlations, which results in the featureless Q dependence for $x \geq 0.66$. Fully understanding the Q dependence and the Zeeman response to the external magnetic field requires further theoretical studies on quantum kagome antiferromagnets.

Despite the intense theoretical interest in the nature of spin fluctuations in a quantum kagome system[5–10,25], experimental studies have been rare owing to the scarcity of good model systems. In this letter, we have presented our studies on $Zn_xCu_{4-x}(OD)_6Cl_2$, which realizes a weakly coupled, spin-1/2, kagome antiferromagnet, carried out using elastic and inelastic neutron scattering with and without an external magnetic field. Our systematic studies of magnetic excitations in $Zn_xCu_{4-x}(OD)_6Cl_2$ with various x enable us to construct a schematic phase diagram as a function of x and temperature (Fig. 1d). Various magnetic phases, such as Néel, valence-bond-solid and liquid and cooperative paramagnetic phases, were identified in different regions of the phase diagram, and the characteristics of their spin fluctuations were investigated. Full understanding of our results requires further theoretical and experimental studies on the quantum kagome system, and the experimental results presented here would serve as a crucial test for any theoretical models.

METHODS

We have made elastic- and inelastic-neutron-scattering measurements without field on 100% deuterated powder samples of $Zn_xCu_{4-x}(OD)_6Cl_2$ with five different Zn concentrations, $x = 0, 0.2, 0.4, 0.66$ and 1. The measurements were made at the NIST Center for Neutron Research using the time-of-flight Disk-Chopper-Spectrometer (DCS), the cold-neutron triple-axis spectrometer SPINS and the thermal triple-axis spectrometer BT9. Experimental configurations that have basically two different energy resolutions were used for our measurements: one set of data was taken up to $\hbar\omega \sim 2.5$ meV with an energy resolution of $\Delta\hbar\omega \sim 0.1$ meV and the other set of data was taken up to $\hbar\omega \sim 15$ meV with a coarser $\Delta\hbar\omega \sim 1$–2 meV. We have also made the measurements with an external magnetic field on $Zn_{0.66}Cu_{3.34}(OD)_6Cl_2$ at the Hahn–Meitner Institut using the triple-axis spectrometer V2. The inelastic data shown in Fig. 2b were obtained from the DCS raw data with empty-can background subtracted. The data still contain non-magnetic signal, especially at very low energies, owing to the instrumental energy lineshape, which is a characteristic of a time-of-flight spectrometer. The magnetic and the non-magnetic component were separated using the detailed balance relation $I(-\hbar\omega, T) = I(\hbar\omega, T)\exp(-\hbar\omega/k_BT)$ (S.-H. Lee, unpublished) and the magnetic components were plotted in Fig. 3b.

Received 16 March 2007; accepted 18 July 2007; published 26 August 2007.

References

1. Anderson, P. W. Resonating valence bonds—new kind of insulator. *Mater. Res. Bull.* **8**, 153–160 (1973).
2. Fazekas, P. & Anderson, P. W. Ground-state properties of anisotropic triangular antiferromagnet. *Phil. Mag.* **30**, 423–440 (1974).
3. Anderson, P. W. The resonating valence bond state in La_2CuO_4 and superconductivity. *Science* **235**, 1196–1198 (1987).
4. Kivelson, S. A., Rokhsar, D. S. & Sethna, J. P. Topology of the resonating valence-bond state—solitons and high-T_c superconductivity. *Phys. Rev. B* **35**, 8865–8868 (1987).
5. Read, N. & Sachdev, S. Large-N expansion for frustrated quantum antiferromagnets. *Phys. Rev. Lett.* **66**, 1773–1776 (1991).
6. Hastings, M. B. Dirac structure, RVB, and Goldstone modes in the kagomé antiferromagnet. *Phys. Rev. B* **63**, 014413 (2001).
7. Park, K. & Sachdev, S. Bond and Néel order and fractionalization in ground states of easy-plane antiferromagnets in two dimensions. *Phys. Rev. B* **65**, 220405(R) (2002).
8. Senthil, T., Balents, L., Sachdev, S., Vishwanath, A. & Fisher, M. P. A. Quantum criticality beyond the Landau–Ginzburg–Wilson paradigm. *Phys. Rev. B* **70**, 144407 (2004).
9. Ran, Y., Hermele, M., Lee, P. A. & Wen, X.-G. Projected wavefunction study of spin-1/2 Heisenberg model on the kagomé lattice. *Phys. Rev. Lett.* **98**, 117205 (2007).
10. Ryu, S., Motrunich, O. I., Alicea, J. & Fisher, M. P. A. Algebraic vortex liquid theory of a quantum antiferromagnet on the kagomé lattice. *Phys. Rev. B* **75**, 184406 (2007).
11. Ramirez, A. P. in *Handbook on Magnetic Materials* Vol. 13 (ed. Busch, K. J. H.) 423 (Elsevier Science, Amsterdam, 2001).
12. Lee, S.-H. *et al.* Emergent excitations in a geometrically frustrated magnet. *Nature* **418**, 856–858 (2002).
13. Shores, M. P. *et al.* A structurally perfect $S = 1/2$ kagomé antiferromagnet. *J. Am. Chem. Soc.* **127**, 13462–13463 (2005).
14. Helton, J. S. *et al.* Spin dynamics of the spin-1/2 kagomé lattice antiferromagnet $ZnCu_3(OH)_6Cl_2$. *Phys. Rev. Lett.* **98**, 107204 (2007).
15. Ofer, O. *et al.* Ground state and excitation properties of the quantum kagomé system $ZnCu_3(OH)_6Cl_2$ investigated by local probes. Preprint at <http://www.arxiv.org/cond-mat/0610540> (2006).
16. Mendels, P. *et al.* Quantum magnetism in paratacamite family: Heading towards an ideal kagomé lattice. *Phys. Rev. Lett.* **98**, 077204 (2007).
17. Zheng, X. G. *et al.* Unconventional magnetic transitions in the mineral clinoatacamite $Cu_2Cl(OH)_3$. *Phys. Rev. B* **71**, 052409 (2005).
18. Zheng, X. G. *et al.* Coexistence of long-range order and spin fluctuation in geometrically frustrated clinoatacamite $Cu_2Cl(OH)_3$. *Phys. Rev. Lett.* **95**, 057201 (2005).
19. Sato, T. J. *et al.* Unconventional spin fluctuations in the hexagonal antiferromagnet $YMnO_3$. *Phys. Rev. B* **68**, 014432 (2003).
20. Nishiyama, M. *et al.* Magnetic ordering and spin dynamics in potassium jarosite: A Heisenberg kagome lattice antiferromagnet. *Phys. Rev. B* **67**, 224435 (2003).
21. Matan, M. *et al.* Spin waves in the frustrated kagome lattice antiferromanget $KFe_3(OH)_6(SO_4)_2$. *Phys. Rev. Lett.* **96**, 247201 (2006).
22. Furrer, A. & Gudel, H. U. Neutron inelastic-scattering from isolated clusters of magnetic ions. *J. Magn. Magn. Mater.* **14**, 256–264 (1979).
23. Lee, S.-H. *et al.* Isolated spin pairs and two-dimensional magnetism in $SrCr_{9p}Ga_{12-9p}O_{19}$. *Phys. Rev. Lett.* **76**, 4424–4427 (1996).
24. Rigol, M. & Singh, R. R. P. Magnetic susceptibility of the kagomé antiferromagnet. *Phys. Rev. Lett.* **98**, 207204 (2007).
25. Levi, B. G. New candidate emerges for a quantum spin liquid. *Phys. Today* **60**, 16–19 (2007).
26. Mizuno, Y. *et al.* Electronic states and magnetic properties of edge-sharing Cu–O chains. *Phys. Rev. B* **57**, 5326–5335 (1998).
27. Tornow, S., Entin-Wohlman, O. & Aharony, A. Anisotropic superexchange for nearest and next-nearest coppers in chain, ladder, and lamellar cuprates. *Phys. Rev. B* **60**, 10206–10215 (1999).

Acknowledgements

We thank D. Khomskii, S. Sachdev and M. Gingras for helpful discussions. S.-H.L. is supported by US DOC through NIST-70NANB5H1152. Activities at NIST were partially supported by NSF through DMR-0454672.
Correspondence and requests for materials should be addressed to S.-H.L.
Supplementary Information accompanies this paper on www.nature.com/naturematerials.

Competing financial interests

The authors declare no competing financial interests.